Journal of Structural Geology 31 (2009) 208–214

Contents lists available at ScienceDirect

Journal of Structural Geology

journal homepage: www.elsevier.com/locate/jsg

A geochemical estimation of fluid flux and permeability for a fault zone in Mugi mélange, the Cretaceous Shimanto Belt, SW Japan

Y. Hashimoto [a,*], A. Nikaizo [a], G. Kimura [b]

[a] Department of Natural Environmental Science, Faculty of Science, Kochi University, Akebonocyo 2-5-1, Kochi 780-8520, Japan
[b] Department of Earth planetary science, Faculty of Science, University of Tokyo, Hongo 7-3-1, Tokyo 113-0033, Japan

ARTICLE INFO

Article history:
Received 2 October 2007
Received in revised form
26 July 2008
Accepted 2 December 2008
Available online 11 December 2008

Keywords:
Hydraulic property
Seismogenic fault
Subduction zone
Accretionary complex
Shimanto Belt

ABSTRACT

The fluid flux and permeability along seismogenic subduction interfaces were estimated roughly based on geological evidences. A decrease in silica from the host rocks to the deformed rocks due to rock–fluid interaction within the fault–fluid system was qualitatively examined. The area under study was the northernmost part of the Mugi mélange in the Cretaceous Shimanto Belt, Shikoku, SW Japan. A fault zone with pseudotachylytes is located at the area as the roof thrust of the Mugi mélange. The pressure–temperature conditions of the fault zone correspond to the depth around the onset of the seismogenic zone along the subduction interface.

On the basis of deformation texture, rocks are classified into three types—mélange, fault breccia, and ultracataclasite. The bulk chemical analysis of the abovementioned rocks was conducted by employing the X-ray fluorescence (XRF) analysis method. The average mass loss from the mélange host rocks to the fault rocks was estimated by the isocon method. In particular, a decrease in silica was observed clearly. Based on the decrease in silica and certain other geological constraints such as the pressure–temperature conditions of fluid, length of the fault, and the duration between deposition and exhumation, the amount of fluid reacting with rocks and the fluid flux were examined roughly. The estimated fluid volume was approximately thousand times the rock volume, and the fluid flux was about 10^{-8}–10^{-6} m/s. Based on the fluid flux and some constraints in temperature pressure conditions of fluid and pressure gradient, the permeabilities of fault zone rocks were estimated, which was approximately of the order of about 10^{-17}–10^{-16} m^2 and about 10^{-16}–10^{-14} m^2 in the fault breccia and ultracataclasite, respectively. While the estimated value of the permeability of the fault breccia is similar to that obtained in laboratory experiments, the estimated value of the permeability of the ultracataclasite is considerably larger than that obtained from laboratory experiments. This probably indicates that the permeability of the ultracataclasite is not constant as observed in the laboratory experiments but can evolve during seismic cycle.

1. Introduction

Subduction zones are one of the largest fault–fluid systems in the world. In particular, a subduction zone with accretionary prisms contains a large amount of sediments that are under thrust to greater depths with a large quantity of fluid within the pore space and mineral phases. Many studies have presented the fluid concentration along faults in shallow to deep accretionary complexes, based on the geophysical and geological evidences. The negative polarities of reflection along the faults are considered to indicate the existence of fluid along the fault (e.g., Park et al., 2002). A chloride anomaly was detected along a shallow decollement in the ODP drilled hole of Leg 190 (e.g., Saffer and Bekins, 1998), which might be caused by the freshening of seawater by smectite dehydration. Cold seepages with shell colonies were detected on the seafloor along the faults exposed at the surface by a submarine explorer (e.g., Le Pichon et al., 1992). Fluid inclusion analyses have been performed on the mineral veins in on-land fossil accretionary complexes; these studies provide some evidences regarding the chemical composition of the fluid and its pressure–temperature conditions along deep subduction interfaces (e.g., Vrollijk et al., 1988; Hashimoto et al., 2002, 2003; Matsumura et al., 2003).

A subduction zone is also the place where some of the world's largest earthquakes occur. Because the fluid pressure affects the effective pressure, thereby weakening the fault strength and frictional resistance, the existence of fluid along the fault is considered to be a significant factor in understanding the fault activities (e.g., Hubbert and Rubey, 1959). However, several studies on the

* Corresponding author.
E-mail address: hassy@cc.kochi-u.ac.jp (Y. Hashimoto).

0191-8141/$ – see front matter © 2008 Elsevier Ltd. All rights reserved.
doi:10.1016/j.jsg.2008.12.001

abovementioned fluid–fault system along subduction zones have provided insufficient quantitative information regarding hydraulic properties. Experimental studies that ought to evaluate the fluid effects on fault weakening have satisfactorily examined hydraulic properties such as permeability and porosity (e.g., Tsutsumi et al., 2004; Song et al., 2004; Wibberley and Shimamoto, 2005). On the basis of hydraulic properties, Wibberley and Shimamoto (2005) suggested that thermal pressurization might be the main weakening process during seismicity. Fluid flux and hydraulic properties are significant constraints in evaluating the extent of fluid effects on fault strength. However, the experimental studies stated above considered the stable properties of rocks and not their dynamic properties.

Recently, pseudotachylyte has been detected within the roof thrust of on-land accretionary complexes, which indicates that the fault was at the seismogenic plate boundary (Ikesawa et al., 2003; Kitamura et al., 2005; Ujiie et al., 2007). The northern most boundary of the mélange zone is recognized as a roof thrust of a underplated accretionary complex. Kimura et al. (2007) suggested that the boundary can be interpreted as an analogue fault of deep strong reflector (DSR) with negative polarity (Park et al., 2002). In this study, we examine the boundary fault containing pseudotachylytes in the Mugi mélange in the Cretaceous Shimanto belt, SW Japan. The Shimanto belt has been reported to provide a large amount of basic data such as depositional and exhumation ages (Ohmori et al., 1997; Kimura et al., 2007), palaeo temperature and pressure conditions obtained from vitrinite reflectance (Ohmori et al., 1997; Matsumura et al., 2003), and fluid inclusion analysis (Matsumura et al., 2003). The degree of rock–fluid interaction has been quantitatively examined by conducting whole-rock chemical analysis (e.g., Grant, 1986; O'Hara and Blackburn, 1989; Goddard and Evans, 1995; Tanaka et al., 2001; Kawabata et al., 2007). In this study, the fluid flux and permeability along the seismogenic fault were estimated by combining the results of the isocon method with geological constraints. This might represent the integration of the hydraulic properties in the pre-, co-, and post-seismic periods along the seismogenic subduction interface in geological time scale.

2. Geological setting and occurrences of the boundary fault of Mugi mélange

The Shimanto belt is distributed along SW Japan parallel to the Nankai Trough (Taira et al., 1988). The Mugi mélange is located in the Cretaceous Shimanto belt, Shikoku island (e.g., Onishi and Kimura, 1995; Ikesawa et al., 2005) (Fig. 1a). The lithofacies of the Mugi mélange are mainly tectonic mélange composed of sandstone blocks surrounded by black shale matrices, minor basalts, tuffs, and hemipelagic shales (Onishi and Kimura, 1995; Ikesawa et al., 2005). The depositional age was newly determined based on the Pb isotope ratio in zircons representing about 60–70 Ma (Kimura et al., 2007; Shibata et al., 2008). The maximum palaeo temperature estimated from vitrinite reflectance was about 180–220 °C (Ohmori et al., 1997; Matsumura et al., 2003). The fluid inclusion analysis revealed the fluid temperature and pressure conditions to be about

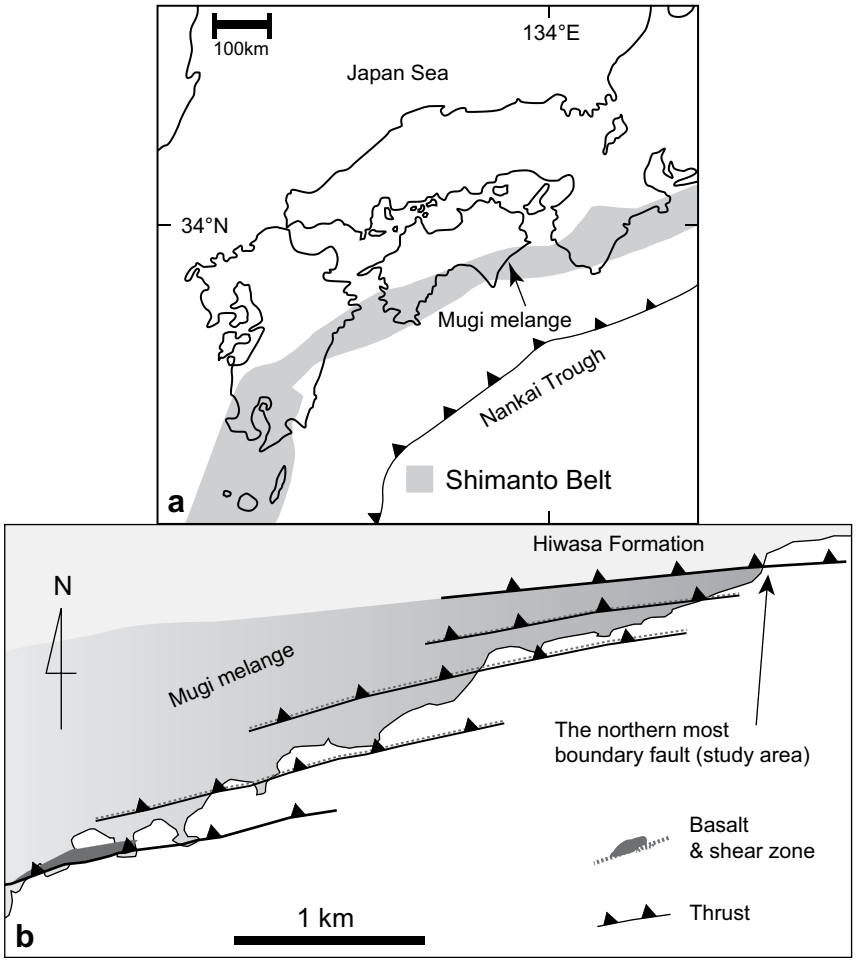

Fig. 1. (a) Distribution of the Shimanto Belt in SW Japan and (b) Schematic map of the Mugi mélange and Hiwasa formation.

160–240 °C and 100–150 MPa, respectively (Matsumura et al., 2003).

At the northernmost part of the Mugi mélange, the boundary fault zone named Minami-awa Fault divides the northern coherent unit of the Hiwasa group and the Mugi mélange (Kitamura et al., 2005) (Figs. 1b and 2a). This fault is interpreted as the roof thrust of the Mugi mélange. The fault zone comprises fault breccia of about 2 m in thickness and a thin (up to a few millimeters) ultracataclasite (Fig. 2b and c). The fault breccia is comprised of black shale and acidic tuff (Fig. 2a and b). Although the fault breccia zone represents a mélange-like texture in the outcrop scale, the deformation mechanism of the zone is cataclastic on the basis of microscopic observation (Kitamura et al., 2005). The fault does not cut the thermal structure estimated from the vitrinite reflectance increasing from the north to the south (Kitamura et al., 2005), which indicates that the fault was formed in a temperature about 180–220 °C (Matsumura et al., 2003; Kitamura et al., 2005). Much quartz, laumontite and calcite veins (less than 1 mm in thickness) are observed mainly parallel to the cataclastic foliations within the fault zone. A pseudotachylyte was detected in the fault zone (Kitamura et al., 2005; Ujiie et al., 2007), suggesting that the roof thrust was a seismogenic fault. The first of the fossil–pseudotachylyte from the on-land accretionary complex is located at the same setting of the fault located at the northernmost part of the mélange zone of the Okitsu mélange, Shikoku, SW Japan (Ikesawa et al., 2003).

In the south of the fault zone, the Mugi mélange is distributed. Quartz and calcite veins are also observed in the mélange zone parallel or subparallel to the mélange foliations. It is difficult to determine the timing of the vein formation both for the mélange zone and the fault zone. Acidic tuff blocks are also observed in the mélange just below (in the southern part) the fault zone (Fig. 2c). The acidic tuff shows a sharp contact with the black shale matrix of the mélange (Fig. 2c). In the same manner, the acidic tuff in the fault zone is also distinctly separated from the black shale domain (Fig. 2a and b). In this study, we carefully collected the black shale in order to avoid it from mixing with the acidic tuff both from the mélange and the fault breccia zones.

Samples were collected both within and outside the fault zone. The samples from the mélange zone were recovered from locations outside the fault zone, but close to the fault zone within 40 m in the south. We defined the mélange outside the fault zone as host rocks. Further, we also classified these fault rocks into two—fault breccia and ultracataclasite.

The fault zone cuts and incorporates the tectonic mélange located in the south of the fault zone, which clearly indicates that the fault zone was formed after the mélange formation.

A microscopic observation of the ultracataclasite represents that small fragments of quartz grains are surrounded by clayey matrices. The diameters of these fragments range approximately from 10 to 700 μm. Some fragments have elongated shapes and the preferred orientation is almost parallel to the strike of the fault (Fig. 2e). Optical microscope observations reveal that the matrices have a homogeneous texture. On the other hand, Si mapping using an electron probe microanalyzer (EPMA) shows the decrease in Si along some paths that are similar to conduits of fluids within the matrices (Fig. 2f).

3. X-ray fluorescence method and results

The X-ray fluorescence (XRF) method was used to examine the whole-rock composition of the major and minor elements for each rock type. The changes in the chemical characteristics from the host rocks to the deformed rocks have been examined by many studies to estimate the mass and volume losses and the fluid–rock ratio in fault zones (e.g., Grant, 1986; O'Hara and Blackburn, 1989; Goddard and Evans, 1995; Tanaka et al., 2001; Kawabata et al., 2007).

The samples were cut into pieces that measured a few cubic centimeters and crushed into millimeter size in a tungstate carbide mortar. Subsequently, the small, visible pieces of sandstone, acidic tuff and mineral veins were carefully removed and the remaining black shales were collected. This procedure was conducted not only for mélange and fault breccia but also for ultracataclasite as much as possible. The number of samples analyzed was 20 for the host rock (mélange in the southern part of the fault zone), 11 for the fault breccia, and 1 for the ultracataclasite. Because the ultracataclasite layer was too thin to be sampled, the number of ultracataclasite samples was very limited. However, the ultracataclasite was sampled from relatively wider area ranging about 50 cm along the thin layer to get enough amount and they mixed as a single sample to be analyzed. Therefore, the data for the ultracataclasite is a kind of a spatial averaged value although the number of the sample is only one. In addition, the sample of ultracataclasite is adjacent to the black shale domains in the fault breccia zone to avoid the mixing of tuff blocks. The ultracataclasite was collected not from surface but from the maximum possible depth within the outcrops in order to obtain the unweathered portion.

The results of the XRF analysis are shown in Table 1. The differences between fault breccia and mélange, and ultracataclasite and mélange with regard to the amounts of elements are represented in the isocon diagram (Fig. 3) (e.g., Grant, 1986; O'Hara and Blackburn, 1989; Goddard and Evans, 1995; Tanaka et al., 2001; Kawabata et al., 2007). We used TiO_2, Al_2O_3 and Nb as the immobile element as the same as Kawabata et al. (2007). Kawabata et al. (2007) examined the immobility of elements in black shale, in the Mugi mélange and then concluded that TiO_2, Al_2O_3 and Nb are immobile elements. The percentage loss or gain of each element is defined as follows:

$$M = \left[\left(\frac{1}{S}\right) - 1\right] \times 100 \quad (1)$$

S is the immobile isocon defined as weight percent of the immobile element in the deformed rocks over that in the host rocks. Practically, the immobile isocon is the slope of the fitting line of the immobile elements in the isocon diagrams (Fig. 3). M is mass loss ratio.

Immobile isocons of 1.0756 and 1.2646 were obtained between the fault breccia and mélange, and ultracataclasite and mélange, respectively (Fig. 3). Using the abovementioned formula, the loss and gain of elements from the host rocks to the deformed rocks can be examined. The changes in the concentrations (%) of each element in each deformed rock from host rock are shown in Table 2.

Because the main component of rocks is silica, the change in silica is the largest. The decrease of silica is clearly observed from the host rocks (mélange) to the fault breccia and the ultracataclasite. Goddard and Evans (1995) described that the quartz dissolution and feldspar alteration can explain the above result. Silica reduction mainly contributes to the change in mass losses (Goddard and Evans, 1995). The values of silica depletion (L_{si}) are obtained as about 7.84 g silica/100 g rocks and about 20.5 g silica/100 g rocks from the mélange to fault breccia and from the mélange to ultracataclasite, respectively by using equation (1). The increasing trends in the contents of MnO and CaO are relatively larger than those of the others because their quantities are small. Fe and K are contained in relatively larger amounts among the other major elements within rocks, except for SiO_2 and Al_2O_3. Fe decreases significantly in the ultracataclasite from the mélange. On the other hand, the fault breccia contains a slightly higher amount of Fe than the mélange. The amount of K increases in the fault

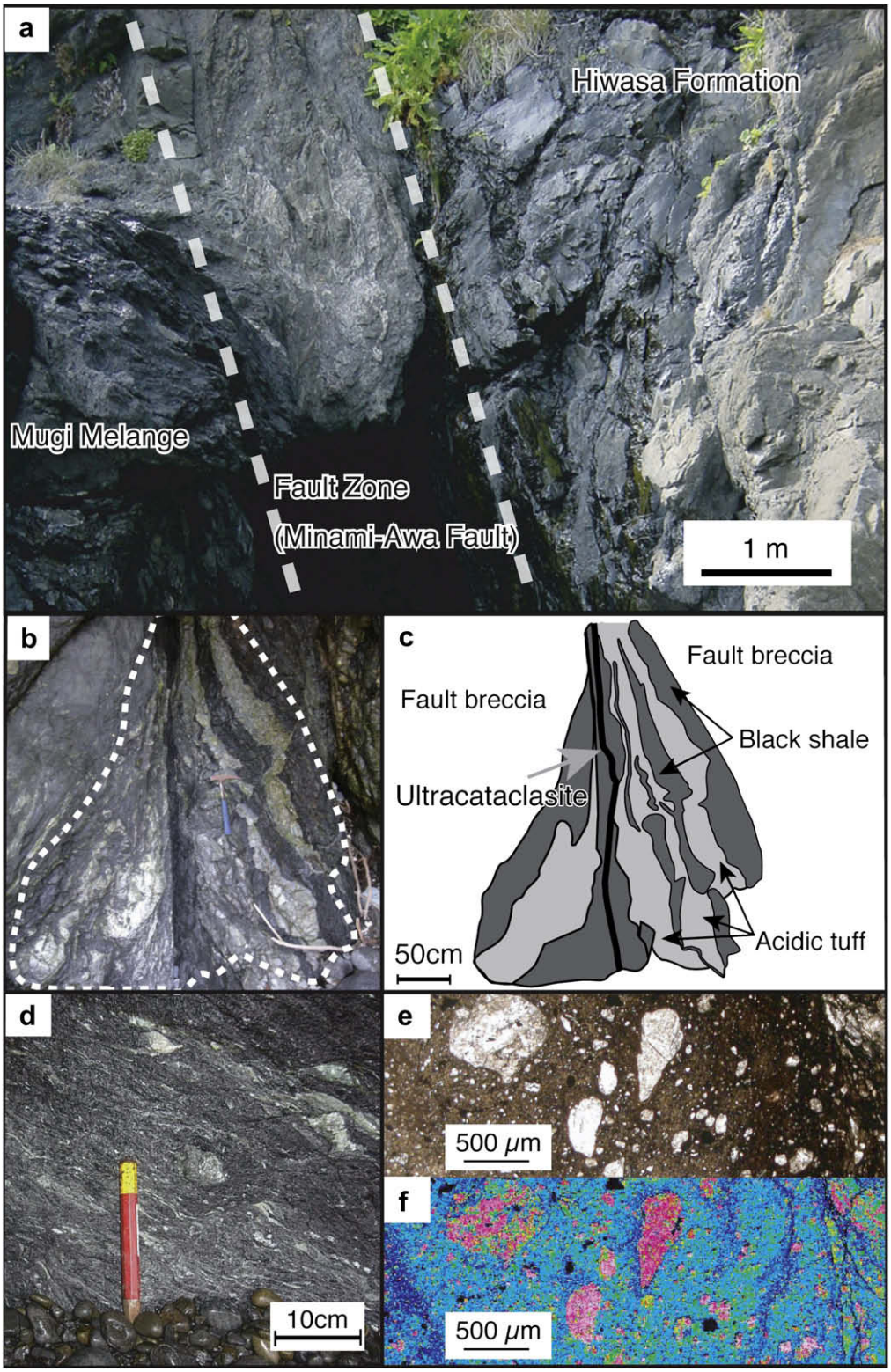

Fig. 2. a) Outcrop of the fault zone (the Minami-Awa Fault), Hiwasa Formation and Mugi Melange. At the bottom of the fault zone, a small cave is shown as a dark part. Mugi mélange is located at the southern part of the Hiwasa formation and the Minami-Awa fault, b) occurrences of the inside of the cave at the bottom of the fault zone, c) a sketch of the outcrop of b, d) the outcrop of the mélange in the southern part of the fault zone (the Mugi mélange). Foliations develops with very denser intervals in the northern part of the Mugi mélange, e) microphotograph of the ultracataclasite under the optical microscope, and f) image of the Si concentration in the area described in Fig 2e by EPMA mapping. The red and blue colors indicate higher and lower concentrations of Si, respectively. (For interpretation of the references to colour in this figure legend, the reader is referred to the web version of this article.)

Table 1
Major and minor element contents analyzed by bulk rock XRF analysis.

	Melange	Fault breccia	Fault gouge
SiO_2(wt%)	69.2	66.0	61.6
TiO_2(wt%)	0.6	0.7	0.8
Al_2O_3(wt%)	15.2	17.7	21.0
Fe_2O_3(wt%)	5.5	5.9	5.8
MnO(wt%)	0.2	0.2	0.3
MgO(wt%)	1.7	1.9	2.1
CaO(wt%)	0.7	0.8	2.1
Na_2O(wt%)	2.3	2.0	1.8
K_2O(wt%)	3.6	4.0	4.3
P_2O_5(wt%)	0.1	0.1	0.1
H_2O^-(wt%)	0.2	0.2	0.2
Total	99.3	99.6	100.1
V (ppm)	93.0	105.2	114.1
Cr (ppm)	43.6	46.7	55.1
Co (ppm)	14.2	19.2	17.6
Ni (ppm)	29.1	35.1	33.7
Rb (ppm)	151.6	173.7	217.1
Sr (ppm)	132.0	102.2	117.4
Y (ppm)	28.2	30.8	41.5
Zr (ppm)	162.2	159.4	213.8
Nb (ppm)	14.6	14.8	15.6
Ba (ppm)	378.8	426.3	618.4
La (ppm)	37.5	38.3	93.1
Ce (ppm)	72.5	76.8	158.8
Th (ppm)	20.0	17.9	14.6

breccia and decreases in the ultracataclasite. The amount of Na_2O also decreases from the host rock to the fault breccia and ultracataclasite (Table 2).

4. Discussion

4.1. The procedure for estimating fluid flux and permeability using silica loss and geological constraints

The procedure for estimating fluid flux is the same as Goddard and Evans (1995) basically. To estimate fluid flux from silica loss and geological constraints, we consider a simple model of fluid–rock interaction along a fault. The fault rocks are assumed to have a similar thickness along the entire length of the fault. Then we can estimate the volume of fault rocks, which is simply a multiplication of the estimated fault length and a unit area. Next we calculate fluid–rock ratio which is the amount of fluid to dissolve the silica from host rocks in a unit volume. The fluid–rock ratio is obtained using the silica loss ratio from the immobile isocon and solubility of silica. The solubility of silica depends on temperature and pressure of fluid. The total volume of fluid to remove the silica from host rocks is calculated from the volume of fault rocks and fluid–rock ratio. The fluid flux is obtained from the total volume of fluid divided by a unit area and duration. In the end, the unit area was canceled. Although the silica dissolution is a time-dependence phenomenon, over geologic time, we assume that the dissolution rate in the fault breccia and in the ultracataclasite will be of the same order of magnitude. The parameters for estimating permeability are fluid flux, viscosity, and pressure gradient. The obtained or assumed parameters are listed in Table 3. In this estimation, the parameters are assumed to minimize fluid flux and permeability to establish a standard for comparison.

In this model, only fluid–rock ratio is concerned to explain the silica loss. Therefore, the origin of fluid, the processes of dissolution and precipitation, and even the distance of fluid flow are not matters for the estimation.

We discuss the fluid flux and the permeability in order magnitude.

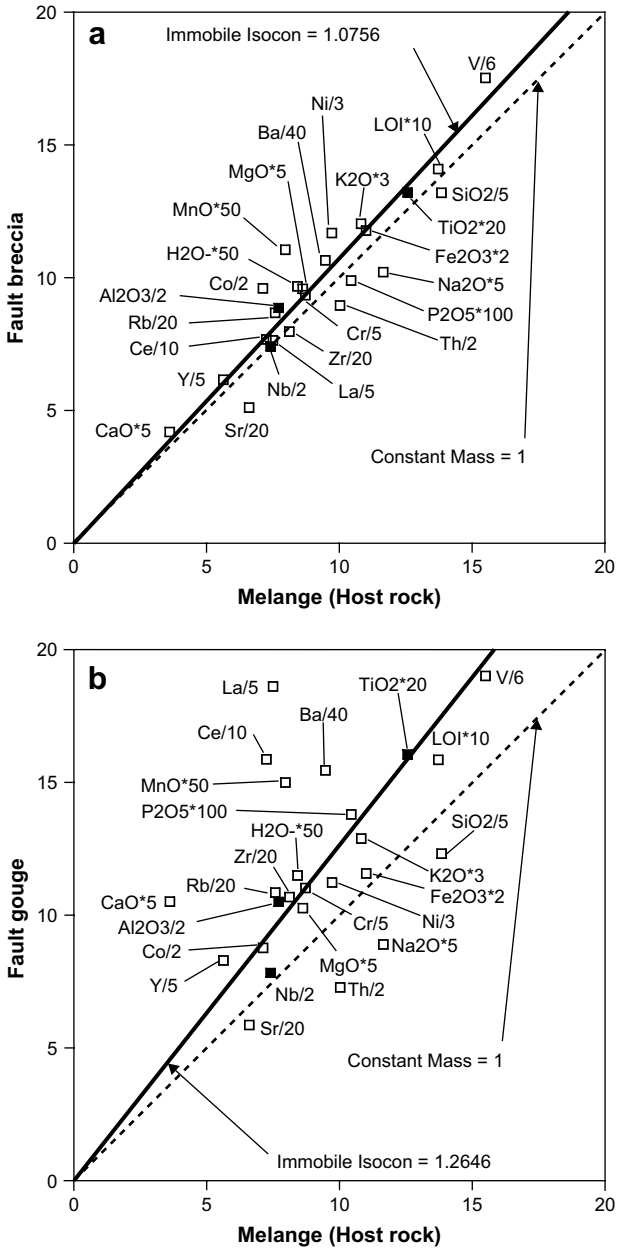

Fig. 3. Isocon diagrams: The amounts of each element were modified to be represented in the graph. The major and minor elements are shown by weight percent and ppm, respectively. Constant mass implies no change in the concentrations of the host and deformed rocks. a) Change in the concentrations of each element from the host rocks to the fault breccia and b) change in the concentrations from the host rocks to the ultracataclasite.

4.2. Estimated fluid flux and permeability along the fault

To estimate the fluid flux, we require some geological constraints such as fault length, duration of fluid flow, and the pressure and temperature of the fluid. We assumed the fault length to be approximately 20 km, which is the Deep Strong Reflector (DSR) length in the seismic profile (Park et al., 2002). Kimura et al. (2007) suggested that the northern boundary fault could be an analogue of the DSR on the basis of the pressure temperature conditions and lithological relationship. The DSR is the strong reflector just above the oceanic basement with a negative polarity, which indicates that the boundary contains significant amounts of fluid (Park et al., 2002). The location of this DSR is in good

Table 2
Percentage changes in the major and minor element contents from the mélange (host rock) to the fault breccia and the ultracataclasite.

	Fault breccia	Fault gouge
SiO_2	−11.3	−29.6
TiO_2	−1.3	1.9
Al_2O_3	8.5	9.1
Fe_2O_3	−0.4	−16.8
MnO	29.1	49.0
MgO	3.4	−5.7
CaO	7.9	130.2
Na_2O	−18.4	−39.6
K_2O	3.5	−5.7
P_2O_5	−11.9	4.5
H_2O^-	6.9	8.0
V	5.2	−3.0
Cr	−0.3	0.1
Co	25.4	−2.5
Ni	11.8	−8.5
Rb	6.6	13.3
Sr	−28.0	−29.7
Y	1.8	16.6
Zr	−8.6	4.2
Nb	−5.5	−15.4
Ba	4.6	29.1
La	−5.1	96.4
Ce	−1.4	73.3
Th	−16.8	−42.5

agreement with the shallow portion of the seismogenic zone in the modern Nankai subduction zone (Park et al., 2002). We considered the temperature and pressure of the fluid to be 200 °C and 150 MPa, respectively estimated form fluid inclusion analysis (Matsumura et al., 2003). The temperature and pressure conditions show also a good agreement with the conditions for DSR. The exhumation age is approximately 43 Ma, as estimated from the fission track age of apatite in the Cretaceous Shimanto belt (Ohmori et al., 1997). The depositional age is approximately 60–70 Ma, as estimated from the ICP-MS of the Pb isotope ratio of zircons (Kimura et al., 2007; Shibata et al., 2008). Based on the differences between the exhumation and depositional ages, the maximum duration of fault activation is assumed to be 30 Ma. The maximum duration makes the estimated fluid flux minimum.

The fluid–rock ratio was examined using the following relationship (Goddard and Evans, 1995)

$$N_w = L_{si}/C^f_{si}(1-s), \quad N_v = N_w\rho^{pr} \tag{2}$$

where N_w is the fluid–rock ratio; N_v, the volumetric fluid–rock ratio; ρ^{pr}, the density of the protolith (2.65 g/cm^3 in this study); L_{si}, the loss of silica calculated as described above; and C^f_{si}, the solubility of silica in the fluid (in grams of silica per grams of solute). C^f_{si} is calculated using the equation proposed by Fournier and Potter (1982). s is the fractional saturation of the fluid with respect to silica. The smaller s indicates that the larger amount of silica can be dissolved and smaller amount of fluid is needed. The s varies 0, 30, 60, 90 and 99% in this study (Table 4). The calculated volumetric fluid–rock ratios are approximately 10^2–10^3 and 10^3–10^4 for the fault breccia and ultracataclasite, respectively (Table 4). By combining these values with the abovementioned geological constraints, the fluid flux (q) can be estimated from the length of the fault, volumetric fluid–rock ratio, and duration of fluid activity using the following equation:

$$q = [20,000(\mathrm{m}) \times N_v]/30(\mathrm{Ma}) \tag{3}$$

As described above, the unit area was canceled in equation (3). Then, fluid fluxes of the order of 10^{-8}–10^{-7} m/s are obtained for both the fault breccia and the ultracataclasite (Table 4). From the fluid flux, we can also calculate the permeability using Darcy's law:

$$q = \frac{-k}{\mu}\nabla P \tag{4}$$

where k, μ, and ∇P are the permeability, viscosity, and pressure gradient vector, respectively. μ is approximately of the order of 10^{-4} Pa s under the estimated temperature–pressure conditions of the fluid in the study area. It is difficult to restrict the pressure gradient. If the fluid pressure ratio is constant along the fault, the pressure gradient should be significantly lower than the lithostatic pressure. A pressure gradient larger than the lithostatic pressure gradient also can be produced when the cracks or fault planes are newly formed. Such a high-pressure gradient is not static. It can be achieved in very short duration as compared to the geological time scale. Therefore, in this study, we use a lithostatic pressure gradient of about 26,000 Pa/m as the maximum static pressure gradient in geological time scale to estimate the minimum permeability. The calculated permeability is approximately of the order of 10^{-17}–10^{-16} m^2 for the fault breccia and 10^{-16}–10^{-14} m^2 for the ultracataclasite (Table 4).

The permeabilities of ultracataclasite and fault breccia have been measured in laboratory experiments on natural samples (e.g., Tsutsumi et al., 2004; Song et al., 2004; Wibberley and Shimamoto, 2005). According to these studies, the permeability of breccia is approximately of the order of 10^{-17}–10^{-16} m^2, which is in good agreement with that of fault breccia observed in this study. On the other hand, the permeability of gouge obtained from the laboratory measurements is approximately of the order of 10^{-20}–10^{-19} m^2, which is significantly lower than that of ultracataclasite observed in this study, even though our calculated permeability is estimated to be the minimum. If the lower permeability of gouge obtained from the laboratory experiments is applied to explain the fluid flux obtained in this study, the pressure gradient must be of the order of about 10^7–10^8 Pa/m with a wide range in s. It is not possible to maintain such a pressure gradient statically on a geological time scale.

Table 3
Parameters for estimation of fluid flux and permeability.

The loss of silica (L_{si})	7.84 g/100 g for fault breccia and 20.5 g/100 g for ultracataclasite
Fault length	20 km
Duration	30 Ma
Solubility (C^f_{si})	0.034 g/100 g
Temperature	200 °C
Pressure	150 MPa
Density of protolith	2.65 g/cm^3
Pressure gradient	26000 Pa/m
Viscosity	10^{-4} Pa s

Table 4
Variations in fluid–rock weight and volume ratios, fluid flux, and permeability with variable silica saturation of fluid.

Sat. (%)	N_w	N_v	Fluid flux (m/s)	Permeability (m^2)
Fault breccia, L_{si} = 7.84 g/100 g				
0	2.29E+02	6.08E+02	1.29E−08	7.03E−17
30	3.28E+02	8.69E+02	1.84E−08	1.00E−16
60	5.74E+02	1.52E+03	3.21E−08	1.76E−16
90	2.29E+03	6.08E+03	1.29E−07	7.03E−16
99	2.29E+04	6.08E+04	1.29E−06	7.03E−15
Ultracataclasite, L_{si} = 20.5 g/100 g				
0	6.00E+02	1.59E+03	3.36E−08	1.84E−16
30	8.57E+02	2.27E+03	4.80E−08	2.63E−16
60	1.50E+03	3.97E+03	8.40E−08	4.59E−16
90	6.00E+03	1.59E+04	3.36E−07	1.84E−15
99	6.00.E+04	1.59.E+05	3.361E−06	1.838E−14

As mentioned above, the simple model is assumed in this estimation. The most significant assumptions are the constant dissolution rate both in fault breccia and in ultracataclasite and an equal thickness of fault rocks along the entire fault length. The fractional saturation of the fluid with respect to silica, *s*, can be converted into a difference in dissolution rate between fault breccia and ultracataclasite. The dissolution rate of ultracataclasite with 0% *s* is 100 times faster than that of fault breccia with 99% *s*. Even in such comparisons, the differences in fluid flux and permeability between the fault rocks are only a single order of magnitude apart (Table 4). If the thickness of ultracataclasite varies or the ultracataclasite is truncated along the fault length, the volume of fluid could be smaller. Then the fluid flux and permeability would be lower in this procedure in total. However, a larger amount of silica loss occurred in the ultracataclasite than in the fault breccia at least in the outcrop studied in this paper. Therefore, a larger permeability is needed to explain the silica loss observed in the outcrop.

This suggests that the larger permeability of ultracataclasite obtained from the geological constraints might be reliable. The permeability of gouge from the laboratory experiments should be a static value because the strain and strain rate in these experiments are very low. On the other hand, the permeability of ultracataclasite obtained from geological evidences must contain variable conditions of strain and strain rate due to events such as earthquakes in the geological time scale. Therefore, the larger permeability of ultracataclasite estimated from this study may indicate an enhanced permeability due to a seismic event and would be significantly larger than that expected under static conditions. The localized silica reduction zone in the ultracataclasite matrices may serve as a conduit related to changes in permeability (Fig. 2e and f). It is reasonable to expect that the permeability of various products of cataclastic deformation will evolve over the course of a seismic cycle. Markers of past fluid flow observed at the outcrop represent a time-averaged history of permeability over the lifetime of the fault. The specific mechanisms by which permeability changes over this time are not fully understood. Although the quantification of permeability in this study remains approximate, it can help provide constraints on the permeability of materials obtained from natural fault systems.

Acknowledgements

We acknowledge the support by Dr. K. Aoike with regard to the XRF analysis and Dr. Y. Yoshimura for extending his help in obtaining the image of EPMA mapping. We also thank Mr. M. Kunth for English modification and discussion. The constructive comments and suggestions by an anonymous reviewer and Dr. C. Rowe are greatly appreciated.

References

Fournier, R.W., Potter, R.W., 1982. An equation correlating the solubility of quartz in water from 25 °C to 900 °C at pressures up to 10,000 bar. Geochim. Cosmochim. Acta 46, 1969–1973.

Goddard, J.V., Evans, J.P., 1995. Chemical changes and fluid–rock interaction in faults of crystalline thrust sheets, northwestern Wyoming, U.S.A. J. Struct. Geol. 17 553–547.

Grant, J.A., 1986. The isocon diagram—a simple solution to Gresens' equation for metasomatic alteration. Econ. Geol. 81, 1976–1982.

Hashimoto, Y., Enjoji, M., Sakaguchi, A., Kimura, G., 2002. P–T conditions of cataclastic deformation associated with underplating: an example from the Cretaceous Shimanto Complex, Kii Peninsula, southwest Japan. Earth Plants Space 54, 1133–1138.

Hashimoto, Y., Enjoji, M., Sakaguchi, A., Kimura, G., 2003. In situ pressure–temperature conditions of a tectonic mélange: constraints from fluid inclusion analysis of syn-melange veins. The Island Arc 12, 357–365.

Hubbert, M.K., Rubey, W.W., 1959. Role of fluid pressure in mechanics of overthrust faulting. Geol. Soc. Am. Bull. 70, 115–166.

Ikesawa, E., Sakaguchi, A., Kimura, G., 2003. Pseudotachylyte from an ancient accretionary complex: evidence for melt generation during seismic slip along a master décollement. Geology 31, 637–640.

Ikesawa, E., Kimura, G., Sato, K., Ikehara-Ohmori, K., Kitamura, Y., Yamaguchi, A., Ujiie, K., Hashimoto, Y., 2005. Tectonic incorporation of the upper part of oceanic crust to overriding plate of a convergent margin: an example from the Cretaceous-early Tertiary Mugi Melange, the Shimanto Belt, Japan. Tectonophysics 401, 217–230.

Kimura, G., Kitamura, Y., Hashimoto, Y., Yamaguchi, A., Shibata, T., Ujiie, K., Okamoto, S., 2007. Transition of accretionary wedge structure around the up-dip limit of the seismogenic subduction zone. Earth Planet. Sci. Lett. 255, 471–484.

Kitamura, Y., Sato, K., Ikesawa, E., Ikehara, O.K., Kimura, Gaku, Kondo, H., Ujiie, K., Onishi, C.T., Hashimoto, Y., Mukoyoshi, H., Masago, H., 2005. Melange and its seismogenic roof decollement: a plate boundary fault rock in the subduction zone – an example from the Shimanto Belt, Japan. TC5012. Tectonics 24 (5), doi:10.1029/2004TC001635.

Kawabata, K., Tnaka, H., Kimura, G., 2007. Mass transfer and pressure solution in deformed shale of accretionary complex: examples from the Shimanto Belt, southwestern Japan. J. Struct. Geol. 29, 697–711.

Le Pichon, X., Kobayashi, K., Kaiko-Nankai Scientific Crew, 1992. Fluid venting activity within the Eastern Nankai Trough accretionary wedge: a summary of the 1989 Kaiko–Nankai results. Earth Planet. Sci. Lett. 109, 303–318.

Matsumura, M., Hashimoto, Y., Kimura, G., Ohmori-Ikehara, K., Enjohji, M., Ikesawa, E., 2003. Depth of oceanic crust underplating in subduction zone- inference from fluid inclusion analysis of crack-seal veins. Geology 31, 1005–1008.

O'Hara, K., Blackburn, W.H., 1989. Volume loss model for trace-element enrichment in mylonites. Geology 17, 524–527.

Ohmori, K., Taira, A., Tokuyama, H., Sakaguchi, A., Okamura, M., Aihara, A., 1997. Paleothermal structure of the Shimanto accretionary prism, Shikoku, Japan: Role of an out-of-sequence thrust. Geology 25, 327–330.

Onishi, C.T., Kimura, G., 1995. Melange fabric and relative convergence in subduction zone. Tectonics 14, 1273–1289.

Park, J.O., Tsuru, T., Tkahashi, N., Hori, T., Kodaira, S., Nakanishi, A., Miura, S., Kaneda, Y., 2002. A deep strong reflector in the Nankai accretionry wedge from multichannel seismic data: implications for underplating and interseismic shear stress release. J. Geophys. Res. 107, doi:10.1029/2001JB000262.

Saffer, D.M., Bekins, B.A., 1998. Episodic fluid flow in the Nankai accretionary complex: timescale, geochemistry, flow rates and fluid budget. J. Geophys. Res. 103, 30351–30370.

Shibata, T., Orihashi, Y., Kimura, G., Hashimoto, Y., 2008. Underplating of mélange evidenced by the depositional ages: U–Pb dating of zircons from the Shimanto accretionary complex, southwest Japan. The Island Arc. 17, doi:10.1111/j.1440-1738.2008.00626.

Song, I., Elphick, S.C., Odling, N., Main, I.G., Ngwenya, B.T., 2004. Hydromechanical behaviour of fine-grained calcilutite and ultracataclasite from the Aigion Fault Zone, Greece. Geoscience 336, 445–454.

Taira, A., Katto, J., Tashiro, M., Okamura, M., Kodama, K., 1988. The Shimanto Belt in Shikoku, Japan-evolution of Cretaceous to Miocene accretionary prism. Mod. Geol. 12, 5–46.

Tanaka, H., Fujimoto, K., Ohtani, T., Ito, H., 2001. Structural and chemical characterization of shear zones in the freshly activated Nojima fault, Awaji Island, southwest Japan. J. Geophys. Res 106, 8789–8810.

Tsutsumi, A., Nishio, S., Mizoguchi, K., Hirose, T., Uehara, S., Sato, K., Tanikawa, W., Shimamoto, T., 2004. Principal fault zone width and permeability of the active Neodani fault, Nobi fault system, Southwest Japan. Tectonophysics 379, 93–108.

Ujiie, K., Yamaguchi, H., Sakaguchi, A., Toh, S., 2007. Pseudotachylytes in an ancient accretionary complex and implications for melt lubrication during subduction zone earthquakes. J. Struct. Geol. 29, 599–613.

Vrollijk, P., Myers, G., Moore, J.C., 1988. Warm fluid migration along tectonic mélanges in the Kodiak Accretionary Complex, Alaska. J. Geophys. Res. 93, 10313–10324.

Wibberley, C.A.J., Shimamoto, T., 2005. Earthquake slip weakening and asperities explained by thermal pressurization. Nature, 436, doi:10.1038/nature03901.